Contents lists available at SciOpen

Food Science and Human Wellness

journal homepage: https://www.sciopen.com/journal/2097-0765

China Food Publishing Co.

Innovative 3D microfluidic intestinal organoid model for assessing cadmium bioavailability in food: implications for enhanced exposure risk assessment

Yan Li[a,b,1], Wen Sun[a,b,1], Qiao Wang[c], Wan Shi[c], Yu Chen[d], Zhiyong Gong[c], Xiao Guo[c,*], Xin Liu[c,*], Yongning Wu[c,e,*]

[a] Key Laboratory of Animal Biological Products & Genetic Engineering, Ministry of Agriculture and Rural, Sinopharm Animal Health Co., Ltd., Wuhan 430023, China
[b] State Key Laboratory of Novel Vaccines for Emerging Infectious Diseases, China National Biotec Group Co., Ltd., Beijing 100024, China
[c] Key Laboratory for Deep Processing of Major Grain and Oil (The Chinese Ministry of Education), College of Food Science and Engineering, Wuhan Polytechnic University, Wuhan 430023, China
[d] Department of Oncology, Xiangya Hospital, Central South University, Changsha 410008, China
[e] NHC Key Laboratory of Food Safety Risk Assessment, China National Center for Food Safety Risk Assessment, Beijing 100021, China

ARTICLE INFO

Article history:
Received 8 June 2023
Received in revised form 20 July 2024
Accepted 2 September 2024

Keywords:
Planar Transwell model
3D intestinal organoid model
Physiological relevance
Cd bioavailability

ABSTRACT

Given the severe toxicity and widespread presence of cadmium (Cd) in staple foods such as rice, accurate dietary exposure assessments are imperative for public health. *In vitro* bioavailability is commonly used to adjust dietary exposure levels of risk factors; however, traditional planar Transwell models have limitations, such as cell dedifferentiation and lack of key intestinal components, necessitating a more physiologically relevant *in vitro* platform. This study introduces an innovative three-dimensional (3D) intestinal organoid model using a microfluidic chip to evaluate Cd bioavailability in food. Caco-2 cells were cultured on the chip to mimic small intestinal villi's 3D structure, mucus production, and absorption functions. The model's physiological relevance was thoroughly characterized, demonstrating the formation of a confluent epithelial monolayer with well-developed tight junctions (ZO-1), high microvilli density (F-actin), and significant mucus secretion (Alcian blue staining), closely resembling the physiological intestinal epithelium. Fluorescent particle tracking confirmed its ability to simulate intestinal transport and diffusion. The Cd bioavailability in rice measured by the 3D intestinal organoid model ((9.07 ± 0.21)%) was comparable to the mouse model ((12.82 ± 3.42)%) but significantly lower than the Caco-2 monolayer model ((26.97 ± 1.11)%). This 3D intestinal organoid model provides a novel and reliable strategy for *in vitro* assessment of heavy metal bioavailability in food, with important implications for food safety and risk assessment.

1. Introduction

Cadmium (Cd) is a highly toxic heavy metal with various adverse health effects[1]. Rice, a major dietary staple, can accumulate Cd from contaminated soils, posing a potential exposure risk[2]. However, not all Cd in rice is available for gastrointestinal absorption, which can lead to an overestimated risk. It has been noted that the intake of toxicants from food should not be assessed merely by their quantity but also by their bioaccessibility and bioavailability[3-4]. Toxicants can be partially released from the food matrix during digestion. The fraction of the toxicant that is mobilized into the digestive juices (chyme) is defined as the bioaccessible fraction[5], while bioavailability refers to the proportion of the bioaccessible toxicants that is absorbed and enters the bloodstream[5]. Recent study have emphasized that the risk of Cd toxicity from rice consumption depends not only on the total Cd

[1] These authors contributed equally.

* Corresponding authors at: College of Food Science and Engineering, Wuhan Polytechnic University, Wuhan 430023, China.
E-mail address: xiaoguo@whpu.edu.cn (X. Guo); liuxinhook@whpu.edu.cn (X. Liu); wuyongning@cfsa.net.cn (Y.N. Wu)

Peer review under responsibility of Beijing Academy of Food Sciences.

SciOpen Publishing services by Tsinghua University Press

http://doi.org/10.26599/FSHW.2024.9250364

content in the grains but also crucially on the concentrations that are bioaccessible and bioavailable[6].

Although *in vivo* human studies are ideal for assessing the bioaccessibility and bioavailability of Cd, practical limitations (cost, time, and ethics) often necessitate the use of *in vitro* models[7]. The human intestinal cell line (Caco-2) is widely employed as a representative model to study toxicant bioavailability[8]. This approach involves seeding Caco-2 cells onto Transwell inserts to establish an intact barrier that mimics the intestinal epithelium[9]. The planar Transwell model has been utilized to evaluate Cd bioavailability in various food matrices, such as rice, pork kidney, and lettuce[6,10]. However, the planar Transwell model has some apparent limitations, including the cells spread predominantly along the horizontal direction of the culture dish and are prone to flattening and dedifferentiation[11-12], which impede the model from simulating the three-dimensional (3D) structure and differentiated cell types of the small intestinal villi. Moreover, the *in vitro* planar Transwell model lacks critical components of the intestinal epithelium, such as goblet cells and the mucous layer (or mucins), which are essential for the absorption of substances within the intestinal cavity[13]. These limitations highlight the need for a more physiologically relevant *in vitro* platform to understand better the bioavailability of Cd or other toxicants in the intestinal environment.

A 3D intestinal cell model called intestinal organoid has been developed to enable more realistic exposure conditions and physiologically relevant developmental processes, providing a more accurate representation of harmful substance absorption within the intestine[14]. For instance, studies have induced Caco-2 cells to form 3D intestinal villus structures in chip devices by applying specific stress forces, better mimicking the actual intestinal structure and physiology[15]. Furthermore, a recent study evaluated the effects of polystyrene nanoplastics in human intestinal organoids, observing polystyrene nanoplastics accumulated in multiple cells, in contrast to the limited accumulation observed in 2D cell lines[16], moreover, a more significant apoptosis (apoptosis rate was close to the results of *in vivo* study) was observed in the human intestinal organoids compared with 2D cell lines[16]. These results suggested that the 2D cell lines may do not accurately reflect the intestinal conditions *in vivo*, leading to an underestimation of the intestinal toxicity of polystyrene nanoplastics. However, no established intestinal organoid model currently exists for assessing Cd bioavailability in rice. This gap in the research leads to an insufficient understanding of Cd bioavailability from rice consumption. Results from the evaluation of Cd bioavailability are critical for accurate risk assessment and the establishment of regulatory limits for Cd in rice.

This study aims to establish a novel organoid-on-a-chip model to evaluate the bioavailability of Cd in rice. Firstly, a Caco-2 organoid model of human small intestinal cancer cells will be cultured on a microchip to closely replicate the 3D structure, mucus production, and absorption functions analogous to those of the small intestinal villi. The physiological relevance of this model will be assessed by evaluating its morphology, markers of differentiated cells, permeability, and structural integrity. Subsequently, the bioavailability of Cd in rice will be compared between the organoid-on-a-chip model and the conventional planar Transwell model. This study will provide important theoretical support for risk assessment and standard setting of Cd levels in rice.

2. Materials and methods

2.1 Sample preparation

Cd-contaminated rice samples were collected from Hubei, China, representing low (Rice-L, (0.091 7 ± 0.002 6) mg/kg), medium (Rice-M, (0.408 4 ± 0.019 5) mg/kg), and high (Rice-H, (0.681 6 ± 0.028 3) mg/kg) pollution levels. A normal rice sample (Rice-N) was also purchased from a supermarket in Wuhan, China. The Rice-N was mixed with a $CdCl_2$ solution (0.4 mg/L) to achieve a Cd content consistent with the Rice-M sample (Rice-N + $CdCl_2$, (0.399 8 ± 0.009 8) mg/kg). All rice samples were cooked with ultrapure water at a water-to-rice ratio of 1:1.5 (*m*/*m*). The cooked samples were then dried at 40 °C, pulverized, and passed through a 100-mesh sieve before being sealed for storage.

2.2 Determination of Cd content

The Cd content in rice samples was determined following a modified protocol based on the previously described[17]. Approximately 0.2 g of each sample (n = 3) was digested with 7.0 mL of concentrated nitric acid (HNO_3). The digestion tubes were allowed to stand overnight at room temperature before being placed in a microwave digestion furnace (CEM Mars 6 240/50, Matthews, NC, USA). The temperature was then increased in steps from 75 °C to 140 °C over 2 h. The digested samples were cooled, diluted with 25 mL of deionized water, and filtered (0.45 μm filters) before analysis by inductively coupled plasma mass spectrometry (ICP-MS, NexION 350X, PerkinElmer Life Science). The digestion and analysis procedures included 3 blank samples and a standard reference material (n = 3, certified reference material GBW10048 (GSB-26), China) for quality assurance and control. The adding standard recovery was (100 ± 5)%.

2.3 Simulated digestion in vitro

An *in vitro* digestion model was modified based on the RIVM method[18] to evaluate the bioaccessibility of Cd. Artificial digestive juices (saliva, gastric juice, duodenal juice, and bile) were prepared, and their compositions are provided in Table S1. Approximately 0.5 g of each rice sample was sequentially digested under the following conditions: mouth (pH 6.2, 7 mL, 5 min); stomach (pH 2.0−2.5, 14 mL, 2 h); small intestine (pH 6.5−7.0, 14 mL duodenal juice + 7 mL bile, 2 h). Finally, the duodenal juice was heated at 90 °C for 5 min to denature the digestive enzymes and then filtered through a 0.22 μm Supor membrane (Corning Inc., NY, USA).

2.4 Assessment of Cd bioavailability in a Caco-2 cell monolayer model

2.4.1 Caco-2 cell culture

The Caco-2 cell line was obtained from Shanghai Zhongqiao Xinzhou Biotechnology Co., Ltd. (Shanghai, China). The cells (passage number 5–15) were cultured in 25 cm^2 flasks using Dulbecco's Modified Eagle's Medium (DMEM, Hyclone, USA) supplemented with 10% (*V*/*V*) fetal bovine serum (FBS, Hyclone),

1% (*V*/*V*) non-essential amino-acid (NEAA), and 1% antibiotics (complete medium). The cells were incubated at 37 °C with 5% CO_2 in a humidified atmosphere, and the medium was changed every 48 h. When the cells reached approximately 80% confluence, they were subcultured with a 7-day passage frequency using 0.25% trypsin-EDTA. To establish the Caco-2 intestinal model, the cells were seeded at a density of 5.0×10^4 cells/cm^2 on Transwell plates (Millipore 12-well Millicell Hangcell Culture Insert, 0.4 μm pore size membrane, PET; Corning Inc., NY, USA). The culture media was changed every 2 days for 21 days to allow the formation of confluent, differentiated cell monolayers.

2.4.2 Caco-2 cell monolayer model exposure

Before the Caco-2 uptake experiment, the growth medium was removed from each culture well, and the cell layer was washed twice with 37 °C DMEM at pH 7. The cellular integrity was checked by measuring trans-epithelial electrical resistance (TEER) using a volt-ohm meter equipped with a chopstick electrode (Millicell ERS-2, Millipore, USA). The apical side of the cell monolayers received 0.5 mL of the filtered duodenal juice from section 2.3, while the basolateral side received 1.5 mL of HBSS. After 2 h of incubation, the solution from the apical chamber and basolateral side was harvested. The bioavailability of Cd in rice samples was calculated using the following equation:

$$\text{Bioavailability (\%)} = \left(1 - \frac{U_{AP} \times V_{AP}}{F_{AP} \times K_{AP}}\right) \times 100 \quad (1)$$

Where U_{AP} is the concentration of Cd on the apical side (mg/L); V_{AP} is the volume of solution on the apical side (mL); F_{AP} is the concentration of Cd in rice samples (mg/kg); K_{AP} is the mass of rice samples added in the transport experiment (kg).

2.5 Assessment of Cd bioavailability in a 3D intestinal organoid model

2.5.1 Design and fabrication of the micro-fluidic chip

The microfluidic chip (model DAX-1) was provided by AIM Biotech (Singapore). The features of this chip, including its material structure, facilitate fluorescence and confocal microscopy imaging and allow for the control and adjustment of various gel substrates, fluid, and chemical gradients. Each micro-fluidic chip has 3 cell culture devices, each consisting of 1 cell gel channel, 2 media channels, and 4 culture-medium chambers. The bottom of the microfluidic chip is made of a porous polymer, which enables gas exchange during cell culture. Different volumes of medium can be added to the 4 culture-medium chambers to generate the fluid shear forces required for cell culture. The cell gel solution is injected into the cell gel channel and incubated for a period to form a 3D gel structure, with the cells evenly distributed and growing in all directions. The fluid shear force generated by the fluid flow can stimulate the cells, inducing their differentiation and improving their physiological relevance.

2.5.2 Construction of 3D intestinal organoid model

A Caco-2 cell suspension ($2.0 \times 10^7 - 3.0 \times 10^7$ cells/mL) was mixed with high-sugar DMEM medium containing fibrinogen (10 mg/mL) and thrombin (100 U/mL) solutions, and then 10 μL of the mixture was injected into the cell gel channel of the microfluidic chip. The construct was incubated at 37 °C for 1 h. Subsequently, 70 μL and 50 μL DMEM medium (containing 20% FBS) were added to the respective culture-medium chambers, generating the vertical fluid shear forces required for cell culture. The DMEM medium was replaced twice daily to ensure sufficient media supplementation.

The growth of the Caco-2 cells was monitored using bright-field microscopy (IX53, Olympus Co., Japan). Once the physiological structure of the Caco-2 cells was characterized, the expression of the tight junction protein ZO-1, cell nuclei, and microvilli were observed through immunofluorescence staining. Caco-2 cells were fixed with 4% (*m*/*V*) buffered formalin, blocked with 5% goat serum, and incubated with primary antibodies against ZO-1 (1:250, ab190085) and microvilli protein (F-actin, 1:250, ab112124, Abcam) at 37 °C for 2 h. After washing, the cells were incubated with Alexa Fluor 488-conjugated secondary antibodies, and cell nuclei were stained with 4′,6-diamidino-2-phenylindole (DAPI, 1:4 000, Life Technologies). Imaging was performed using a confocal microscope (IX81, Olympus Co., Japan) with 405 and 488 nm lasers.

To further evaluate the physiological relevance of the constructed 3D intestinal organoid model, the presence of mucus was assessed. The small intestine secretes mucus to maintain intestinal functions, including maintaining intestinal mucosal homeostasis and regulating microbial-host immune responses[19]. Caco-2 cells were fixed with 4% (*m*/*V*) buffered formalin, washed with PBS, and stained with Alcian blue solution (pH 2.5) for 12 h. Bright-field microscopy was used to capture the images.

Finally, the permeability and structural integrity of the 3D intestinal organoid model were verified. Fluorescent particles (7 μm in size) were diluted 100-fold in PBS and added (20 μL) to the 2 culture-medium chambers connected to the same medium channel. The flow of the fluorescent particles was observed using a fluorescence microscope (IX53, Olympus Co., Japan).

2.5.3 3D intestinal organoid model exposure

Before assessing Cd uptake in the 3D intestinal organoid model, the growth medium was removed from each culture-medium chamber, and the cell layer was washed twice with 37 °C HBSS at pH 7. The 2 culture-medium chambers connected to the same medium channel were filled with 20 μL of 37 °C filtered duodenal juice from section 2.3. The other 2 culture-medium chambers connected to the same medium channel were filled with 50 μL of 37 °C HBSS (defined as the lower chambers). The cells were then incubated at 37 °C with 5% CO_2 in a humidified atmosphere, and the medium was changed every 20 min. After the formation of the 3D intestinal organoid, the duodenal juice from section 2.3 was continuously introduced into the device at a low flow rate of 30 μL/L, as reported by Schepers et al.[20] for liver-on-a-chip applications. This low flow rate was maintained throughout the differentiation and culture period. Specifically, 10 μL of liquid was collected from the two lower chambers, and then 10 μL of 37 °C preheated intestinal juice was added to the 2 upper chambers. This process was repeated 6 times, after which the solutions from the upper and lower chambers were collected for Cd content determination. The bioavailability of Cd in rice samples was calculated using the following equation:

$$\text{Bioavailability}\ (\%) = (1 - \frac{m_t}{S_w \times S_m}) \times 100 \quad (2)$$

Where S_w is the concentration of Cd in the rice sample (mg/kg); S_m is the mass of intestinal juice added to the upper chambers (kg); m_t is the total amount of Cd (mg) in the upper and lower chambers after absorption.

All animal experiments in this study were conducted in accordance with the principles of animal welfare and were approved by the Animal Ethics Committee of Research unite.

2.6 Characterization of intestinal microvilli and crypt structures in mice

Male C57BL/6N mice 4 weeks of age were used to perform the characterization of intestinal microvilli and crypt structures. The mice were housed in rearing cages under a 12 h light/dark cycle and (22 ± 2) °C temperature and were given access to mouse chow and Milli-Q water *ad libitum*. All animals were fed in the laboratory animal center of Huazhong University of Science and Technology, and the Institutional Animal Care and Use Committee approved the whole procedure of animal experiments. Animal care complied with the Guidelines for the Care and Use of Laboratory Animals. After acclimation for 1 week, mice were sacrificed after anesthesia, and jejunum tissues were collected and fixed in 4% paraformaldehyde. Subsequently, 4–5 μm sections were obtained and subjected to immunofluorescence according to previous study[21].

For dewaxing, the sections were placed in xylene I for 15 min, xylene II for 15 min, and 100% ethanol I, 100% ethanol II, and 95%, 80%, and 70% ethanol for 5 min each. After dewaxing, the rehydrated sections were incubated with Tris-EDTA (pH 9.0) for 25 min under heating in a microwave oven for antigen retrieval. After the deactivation of endogenous peroxidases, the sections were treated with 1% Triton-X 100 and blocked with 10% goat normal serum before incubation with primary antibodies at 4 °C overnight. The primary antibodies were microvilli protein (F-actin, 1:250, Abcam ab112124) and anti-HES1 (Santa Cruz Biotechnology, USA). Alexa-488-conjugated antibodies (Abcam, UK) were used for immunofluorescence staining. Imaging was performed using a confocal microscope (IX81, Olympus Corp., Japan) with 488 nm lasers.

2.7 Statistical analysis

Data are expressed as the mean ± standard deviation (SD). The software OriginPro 2019b (OriginLab Co., MA, USA) and GraphPad Prism 8.0 (GraphPad Software Inc., CA, USA) software were used for graphing and mean difference analysis. The *P*-values were calculated using Student's *t*-test, and the statistical significance threshold was set at $^*P < 0.05$ and $^{**}P < 0.01$.

3. Results and discussion

3.1 Growth of Caco-2 cells in Transwell chamber and Cd bioavailability in the Caco-2 cell monolayer model

The structure of the Transwell chamber and the growth and distribution of Caco-2 cells in the Transwell chamber are shown in Fig. 1A. The space above the Transwell chamber was defined as the apical side (AP), and the space below the Transwell chamber was defined as the basal side (BL). As Caco-2 cells were initially seeded on the AP of the Transwell chamber, they were uniformly distributed on the porous polyester transparent membrane. After 21 days of culture, the Caco-2 cells grew and differentiated into a dense monolayer epithelial cell structure.

The morphology of Caco-2 cells was observed under a bright-field optical microscope, as shown in Fig. 1B. At the beginning of inoculation, Caco-2 cells were uniformly distributed. On days 3 and 8,

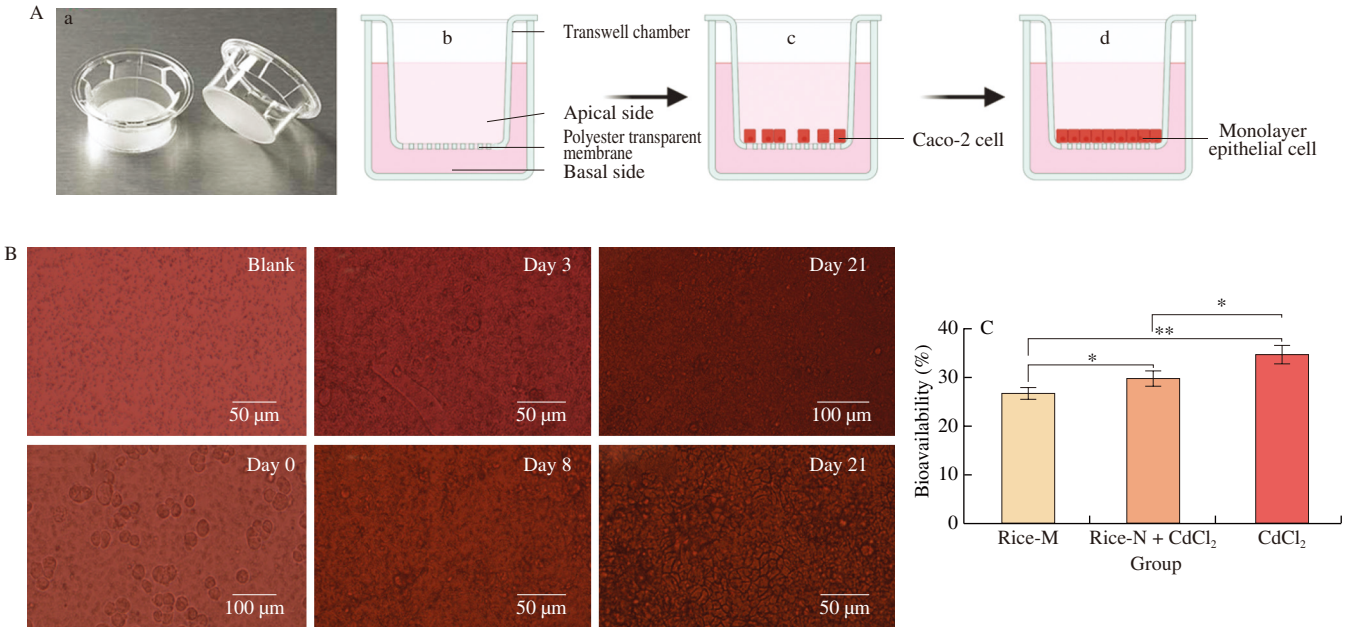

Fig. 1 Characterization of Caco-2 cell growth in a Transwell chamber and Cd bioavailability in Caco-2 cell monolayer model. (A) The (a) picture and (b) diagram of Transwell chamber, (c) growth diagram of Caco-2 cells seeded and (d) cultured for 21 days. (B) Morphological changes of Caco-2 cells. (C) Bioavailability of Cd in different samples. $^{**}P < 0.01$, $^*P < 0.05$.

the number of Caco-2 cells increased significantly, and the cells became flat and irregular in shape, indicating rapid growth and the formation of a planar membrane structure. On day 21, the Caco-2 cells were very densely distributed, with no gaps between cells and clear boundaries, suggesting the formation of tight connections between cells[22]. Some small "clumps" were observed, indicating that the Caco-2 cells had secreted a small amount of mucus.

TEER measurement was used to confirm the integrity of the cellular barrier before studying transepithelial passage of ions, chemicals, or drugs. In this study, after 21 days of culture, the TEER value of Caco-2 cells reached 600 Ω/cm^2. It has been reported that TEER value ≥ 200 Ω/cm^2 can be considered indicative of a tightly connected and relatively complete cell monolayer[23], and a model with TEER values > 250 Ω/cm^2 during differentiation can be used for intestinal absorption studies[24]. Therefore, it can be concluded that the Caco-2 cells had formed a complete and dense intestinal monolayer epithelial cell structure after 21 days of growth and differentiation in the AP of the Transwell compartment.

The *in vitro* bioavailability of Cd refers to the extent to which Cd is released from the food matrix and subsequently absorbed by Caco-2 cells after simulated gastrointestinal digestion[25]. As shown in Fig. 1C, the bioavailability of Cd from the Rice-N + $CdCl_2$ group ((30.04 ± 1.49)%) was significantly ($P < 0.05$) higher than that of the Rice-M group ((26.97 ± 1.11)%), indicating that inorganic Cd was more readily absorbed by the small intestine compared to Cd from the rice matrix. The bioavailability of the $CdCl_2$ group ((35.04 ± 1.63)%) was the highest among all groups, suggesting that the rice matrix significantly affected Cd bioaccessibility *in vitro*. Previous studies have reported that the bioavailability of Cd was affected by the chemical composition of rice, positively correlated with calcium and amylose content, but negatively correlated with the concentrations of sulfur, phosphorus, phytic acid, and crude protein[26], higher concentrations of Ca, Fe, or Zn decreased the bioavailability of Cd[27]. Moreover, essential bivalent metal ions in the rice matrix, such as Fe^{2+}, Mn^{2+}, Zn^{2+}, and Cu^{2+}, may compete with Cd for binding to transporter molecules on the apical side of the small intestine epithelium, leading to a lower absorption rate or similar bioaccessibility of Cd compared to these essential bivalent metal ions[28-29].

3.2 Differentiation and formation of 3D intestinal organoid model

3.2.1 Formation of 3D intestinal organoid model in microfluidic chip

The microfluidic chip device is depicted in Fig. 2. Different volumes of medium were added to the culture medium chambers on different sides, creating fluid shear forces (Fig. 2A). After the Caco-2 cell-containing gel solution was injected into the cell gel channel and incubated, the cell density within the gel increased (Fig. 2B). The fluid shear force provided stimulation to the Caco-2 cells, and after 96 h of incubation, the cells formed a fluctuating epithelial cell structure (Fig. 2B). The Caco-2 cells were confined within the chip throughout the growth process and subsequently differentiated into 3D intestinal organoids, enabling in situ tracking and real-time imaging. Furthermore, the shape and dimensions of the cell gel channel efficiently prevented the fusion of adjacent spheroids during culture, overcoming the limitations of traditional suspension culture approaches.

3.2.2 Formation of tight junction and development of brush border and microvilli

To evaluate the growth of intestinal organoids within the microfluidic chip, we examined the tissue morphology of the organoid during the 96-h culture period. The changes in organoid shape over time are shown in Fig. 3A, spontaneous intestinal morphogenesis was achieved on the chip. Initially, the seeded Caco-2 cells were uniformly distributed in the gel channel and exhibited a circular morphology. After 48 h incubation, a condensation of epithelial cells was sporadically found across the microchannel, indicating the cells had formed a wavy structure[30-31]. After 96 h of incubation, the continuous protrusion of 3D epithelial cell layers was observed, indicating the cells had developed a more pronounced wavy structure[30-31], resembling the fold structure of small intestinal epithelium cells *in vivo*. The small intestine *in vivo* is characterized by ring-like folds and protruding goblet cells in the lumen[32].

The tight junction protein ZO-1 expression is a key characteristic of the intestinal epithelium. As an essential part of the tight junctional

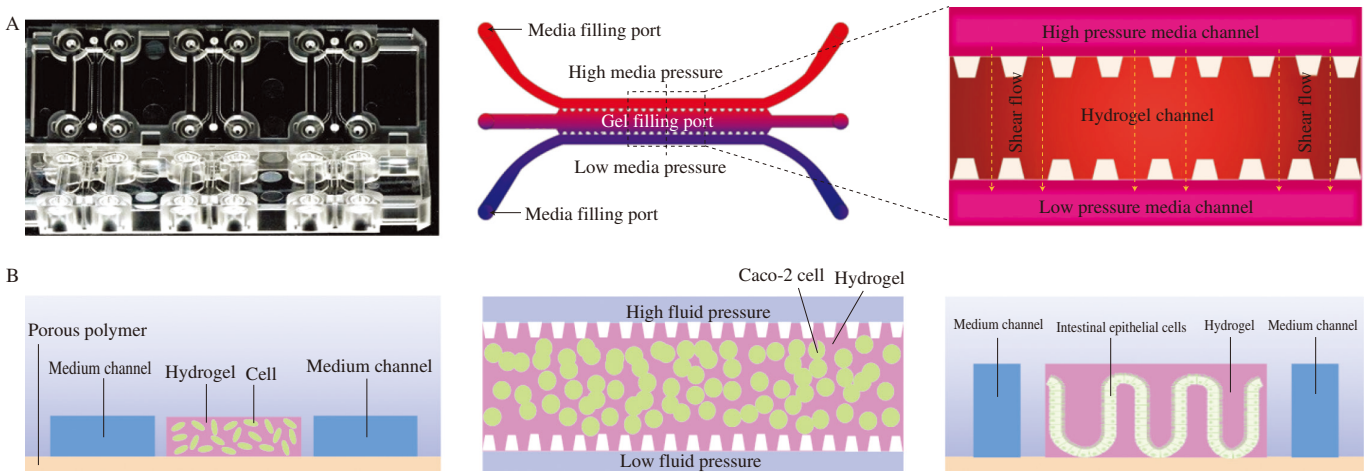

Fig. 2 Schematic diagram of 3D intestinal organoid model from Caco-2 using a microfluidic chip. (A) The appearance and configuration of the microfluidic chip. (B) Schematic diagram of the procedures of differentiation and generation of 3D intestinal organoid from Caco-2 on cell gel channel of chip.

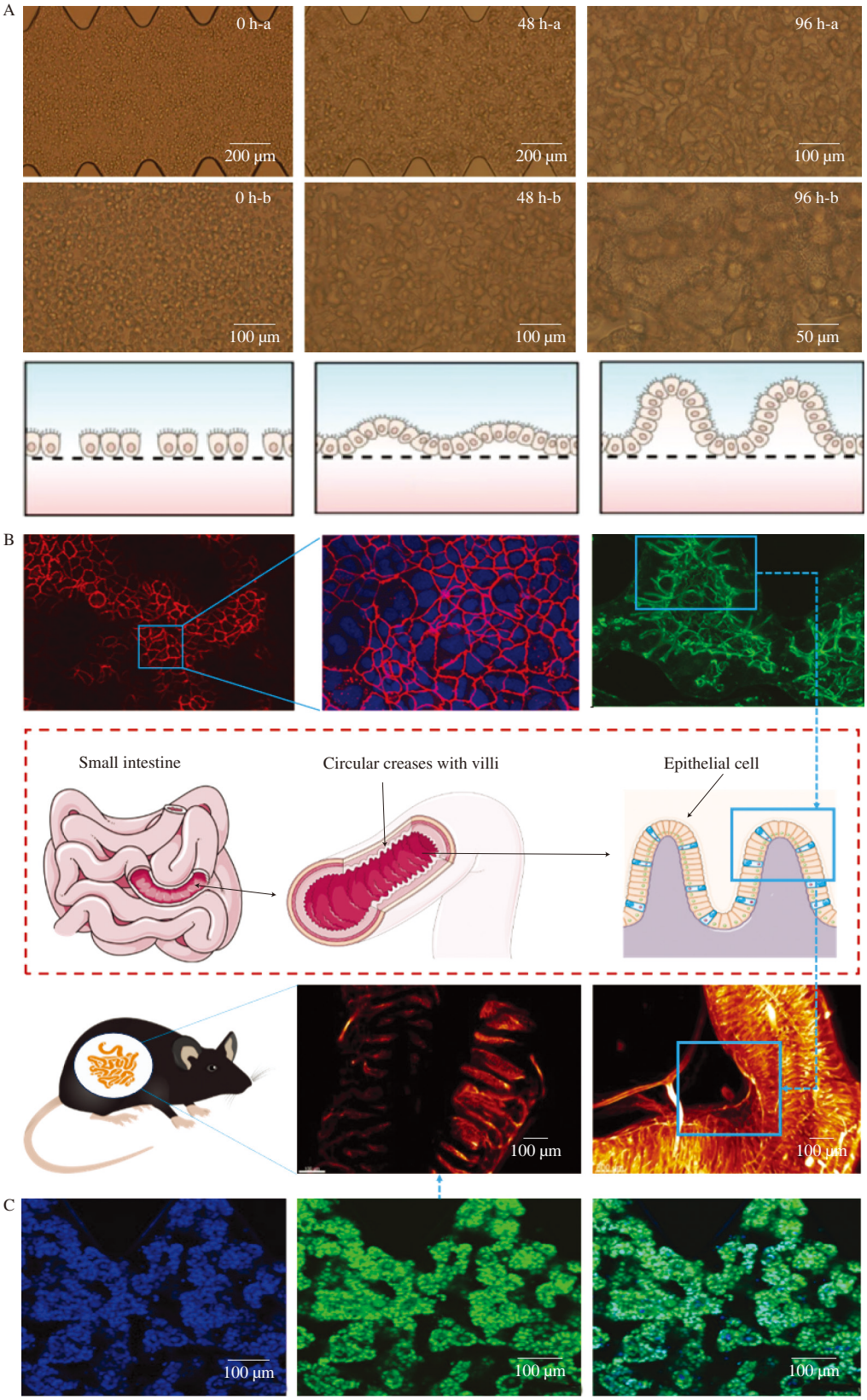

Fig. 3 Characterization of Caco-2 differentiation into intestinal organoid in the micro-fluidic chip. (A) Tissue morphology of the intestinal organoid during the 96-h incubation period (0, 48, and 96 h). Lowercase a-b represented the images observed at low magnification and high magnification, respectively. At the bottom were schematics depicting the cells forming a wavy structure and the *in vivo* intestinal epithelial cell morphology. (B) Immunofluorescence confocal visualization of the tight junction protein ZO-1 (red) the continuous brush-border membrane labeled for F-actin (green) in a horizontal *en face* view of the established 3D intestinal organoid model. At the bottom were immunofluorescence confocal visualization of the intestinal microvilli and crypt structures in mice. (C) Immunofluorescence confocal visualization of the nucleus (blue) and the microvilli proteins (green). Microvilli are distributed on the surface of each small intestinal epithelial cell, so the distribution pattern of microvilli proteins in the images is similar to that of small intestinal epithelial cell. Image on the right was a superposition of the 2 images.

complex, ZO-1 is closely involved in regulating the permeability of the intestinal epithelium[33]. Immunofluorescence staining revealed a confluent epithelial monolayer with well-developed tight junctions in the micro-fluidic chip (Fig. 3B), consistent with the observations of differentiated human Caco-2 cells exhibiting a 'wire fencing-like' organized structure, indicative of tight junction formation[34]. Furthermore, as shown by the blue arrow, the immunofluorescence staining confirmed the intestinal crypt structure of the organoid (Fig. 3B). This was very similar to the intestinal crypt structure that we had observed in the mouse (Fig. 3B). The typical features of the crypt structure are that deformation of intestinal epithelium through apical membrane invagination form T-shaped membrane invaginations (T-folds)[35]. The "wire fencing-like" structure shows the flat state of the cell, while the "intestinal crypt" structure shows the 3D state. During intestinal development, intestinal epithelial cells gradually developed from the initial flat state to the stereoscopic state[35]. It was reported that, in mice, intestinal crypt formation was initiated from the first week after birth, but in humans, intestinal crypt formation has occurred in early gestation (weeks 11–12)[36]. Before that, cells were arranged in a flat sheet, and there is no obvious crypt-like structure[37].

The microvilli, a component of the intestinal brush border, are characterized by villous proteins[38]. As seen in Fig. 3C, the villous proteins were densely distributed (green) within the 3D intestinal organoid model, indicating the formation of many microvilli. As shown by the blue arrow, the distribution of microvilli in intestinal organoids differs slightly from that observed in the mouse intestine (Fig. 3B). Current organoid culture systems do not completely mimic the complex growth environment of the *in vivo* intestine, leading to certain tissue differences. Intestinal organoids primarily consist of intestinal epithelium and lack essential components such as connective, muscular, and neural tissues. Furthermore, they do not contain blood vessels, lymphatic vessels, or support neurogenesis, and are devoid of immune cells and smooth muscle cells[39]. Additionally, variations in cell source and culture conditions affect the structure of organoids. At present, the diversity of cell sources and the lack of standardization in culture techniques contribute to substantial variability in research findings[40]. The extent of microvilli development can be further investigated using scanning electron microscopy, as reported by Przybylla et al.[41].

3.2.3 *Mucus secretion and intestinal transport/ diffusion*

Mucus secretion is a key characteristic of the intestinal epithelium. The mucus layer acts as an important physical barrier in the human body, separating the intestinal bacteria from the epithelial surface[42]. Additionally, the mucus can facilitate the diffusion of substances that reach the intestinal epithelium along the gut wall[43]. Therefore, the mucus secretion of the Caco-2 cells was measured using Alcian blue staining at different time points, with the blue area representing the mucus. As observed in Fig. 4A, the staining indicated significant mucus secretion on the surface of the Caco-2 cell layer within the microfluidic chip. The presence of this mucus layer demonstrates the physiological functions of the 3D intestinal organoid *in vitro*. In contrast, no mucus was found in the Caco-2 cell monolayer model. Previous studies have reported the construction of a gut-mucus system by coating cultured intestinal cells with mucin, the main component of the intestinal mucosal layer, to simulate the physiological environment[44]. Compared to this approach, the advantage of the current study is that the constructed 3D intestinal organoid model can independently differentiate and exhibit the mucus secretion function. Fig. 4B shows the distribution of fluorescent particles loaded into the 3D intestinal organoid model. Over time, some fluorescent particles passed through the model and entered the media channels on the other side, while some particles remained within the organoid. These results indicate that the microfluidic chip used in this experiment can simulate intestinal transport and diffusion. Overall, the comprehensive analysis suggested the efficient differentiation of intestinal epithelial cells and the key functional features of the intestine in the microfluidic chip model.

3.3 *Cd bioavailability in 3D intestinal organoid model*

As shown in Fig. 5, the average bioavailability of Cd in rice in 3D intestinal organoid model was (9.07 ± 0.21)%, which is similar to that in the mouse model ((12.82 ± 3.42)%, data came from our

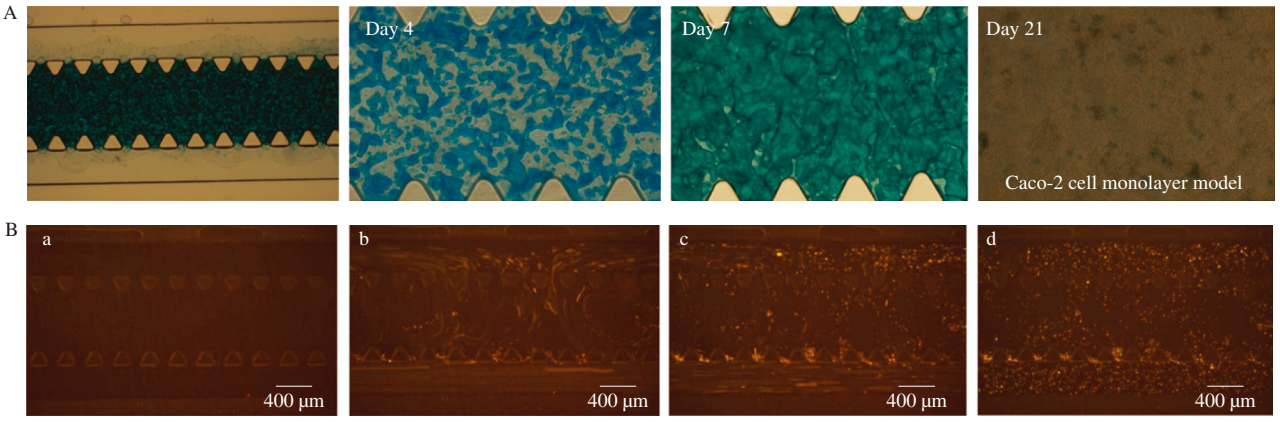

Fig. 4 Physiologically relevant of the 3D intestinal organoid model (mucus secretion and intestinal transport and diffusion function). (A) Alcian blue staining showed the mucus distribution. (B) Migration of fluorescent particles. The lowercase a-d were arranged according to the loading time of fluorescent particles, a-without fluorescent particles, b-0 min, c-10 min, d-20 min.

previous study[10]) but significantly lower than that in the Caco-2 cell monolayer model ((23.72 ± 0.78)%, data came from our previous study[10]). These results indicated that the absorption of Cd in rice in the 3D intestinal organoid model was very close to the *in vivo* scenario but markedly different from the 2D cell culture model. The intestinal absorption of Cd is achieved by means of several transporters such as DMT-1 or Ca-channels[45]. It was reported that 2D cell lines can be induced by Cd to express more transporters[46], this may explain the average bioavailability of Cd in rice in 3D intestinal organoid model was significantly lower than that in the Caco-2 cell monolayer model. In the control group, the bioavailability of $CdCl_2$ in the 3D intestinal organoid and mouse models was similar to that of the Cd in rice, indicating the different bioavailability of Cd in rice in these models could not be attributed to the effect of rice substrate. Structural and functional evaluation of the 3D intestinal organoid model demonstrated that they were highly representative of the physiological structure and properties of the small intestine *in vivo* (Figs. 3 and 4), which may explain why the bioavailability of Cd in this model was very close to the mouse model.

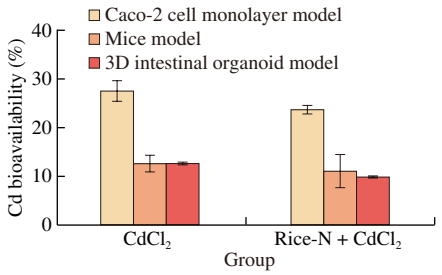

Fig. 5 Bioavailability of Cd in rice in different models.

Previous studies have analyzed the correlation between the bioaccessibility of heavy metals in food substrates (including rice) during *in vitro* simulated gastrointestinal digestion and their bioavailability *in vivo* (mouse model)[47-49], aiming to predict *in vivo* bioavailability through *in vitro* bioaccessibility. However, parameters (e.g., pH and enzymes) of the simulated digestive solution and the type of food substrate significantly impacted the bioaccessibility of heavy metals[49-50], limiting the reliability of using bioaccessibility to predict *in vivo* bioavailability.

The 3D intestinal organoid model constructed in this study can directly reflect Cd's real bioavailability *in vivo*, without being affected by the rice substrate. This represents a meaningful attempt that provides a new perspective and important reference for accurately predicting the *in vivo* bioavailability of heavy metals in food matrices. Furthermore, the bioavailability (9.07%) obtained in this study was used to estimate the daily intake of Cd for different countries. As shown in Table 1, when taking bioavailability into consideration in the estimation, we found that the daily Cd intake was reduced from 4.6−34.6 to 0.42−3.14 μg/day. Calculation of the daily Cd intake on the basis of its total concentration overestimated the Cd exposure by 11.03-fold, as compared with that calculated on the basis of Cd bioavailability. Moreover, the estimated Cd intake from diets for adults on the basis of bioavailable Cd contributes to 1.95%−14.66% of the TDI value recommended by the EFSA.

Table 1
Total and bioavailable values of estimated daily intake of Cd.

Country	Dietary Cd intake (μg/day)[a]	Bioavailability adjusted (μg/day)	Overestimation fold	Contribution rate (%) for TDI[b]
Bangladesh	34.6	3.14	11.03	14.66
Japan	26.4	2.39	11.03	11.19
Spain	19.1	1.73	11.03	8.10
Italy	18.9	1.71	11.03	8.01
Chile	18.1	1.64	11.03	7.67
China	17.3	1.57	11.03	7.33
Ireland	16.9	1.53	11.03	7.16
Hungary	16.2	1.47	11.03	6.87
Belgium	16.1	1.46	11.03	6.82
Lebanon	15.8	1.43	11.03	6.70
France	15.3	1.39	11.03	6.48
Sweden	15.2	1.38	11.03	6.44
Latvia	14.7	1.33	11.03	6.23
Korea	14.5	1.32	11.03	6.15
The Netherlands	14.4	1.31	11.03	6.10
United Kingdom	14.2	1.29	11.03	6.02
Czech Republic	13.8	1.25	11.03	5.85
Denmark	13.5	1.22	11.03	5.72
Canada	13.2	1.20	11.03	5.59
Finland	13.0	1.18	11.03	5.51
Germany	12.9	1.17	11.03	5.47
US	4.6	0.42	11.03	1.95

Note: [a] Data from the report of Zhao et al.[51]. [b] TDI, tolerance daily intake value set by European Food Safety Authority (EFSA) in 2014 at 21.4 μg/day. Assuming a body weight of 60 kg.

The 3D cell culture models, such as organoids, have emerged as superior alternatives to traditional 2D monolayer cultures for studying human development and disease. Organoids possess the ability to self-organize into miniaturized, yet functional, versions of their tissue of origin, thereby more accurately recapitulating the complexity and physiology of the original organ[52].

The present study demonstrates the utility of 3D Caco-2 cell-derived intestinal organoids as a more representative *in vitro* model of human intestinal tissue compared to conventional 2D cultures. Although the intestinal organoids do not yet recapitulate all of the complex structures and cellular interactions associated with the different regions of the intestine (e.g., jejunum, duodenum, ileum, and colon), they contain the specific cell types found in the small intestine, including goblet cells and brush border cells, and exhibited intestine-like structural features (Fig. 3). This suggests that 3D intestinal organoids can serve as valuable basic and translational research tools.

Organoid-based models have successfully studied various diseases and screened new therapeutic compounds[53]. The ability of these 3D structures to faithfully mimic human organ development, morphology, and physiology in a manner akin to *in vivo* conditions has been well-documented[54]. The present study further extends the application of intestinal organoids to the investigation of cadmium absorption, demonstrating their versatility as innovative research platforms.

Despite the extensive research conducted on intestinal chips, their primary applications remain largely focused on drug absorption and activity evaluation[31,55-58]. The uniqueness of this study lies in our innovative application of intestinal chips for assessing the bioavailability of heavy metals, thereby providing a novel perspective on food safety evaluation. This exploration aims to foster a more comprehensive understanding of the potential impacts of heavy metals

on human health. Furthermore, we have successfully developed a three-dimensional intestinal organoid featuring a microvilli structure, a first in the existing literature, achieved through precise control of fluid pressure and cultivation conditions. Our research further posits that traditional planar models assessing the bioavailability of heavy metal cadmium may lead to an overestimation of food safety risks, underscoring the importance of evaluation methods and providing critical insights for a deeper understanding of the potential health impacts of heavy metals. In summary, our study addresses a significant gap in the existing literature, emphasizing the necessity and urgency of employing more precise models for heavy metal risk assessment.

4. Conclusion

This study introduced a 3D intestinal organoid model to investigate the bioavailability of Cd in rice. Constructed on a microfluidic chip, this biomimetic platform enabled Caco-2 cells to form a compact, wave-like intestinal epithelial layer structure. Compared to conventional *in vitro* Caco-2 cell monolayer models, the 3D intestinal organoid system developed in this study more accurately mimicked the physiological intestinal microenvironment and function. Furthermore, the 3D intestinal organoid model directly reflected the *in vivo* bioavailability of Cd in rice, without the confounding effects of the rice substrate. This innovative model offers a novel strategy for reliable assessments of the *in vivo* bioavailability of heavy metals in food matrices. The findings from this study demonstrate the utility of 3D intestinal organoids as a valuable tool for improving the evaluation of *in vivo* bioavailability, with significant implications for food safety and risk assessment.

Declaration of competing interest

Yongning Wu is an editorial board member for *Food Science and Human Wellness* and was not involved in the editorial review or the decision to publish this article. The authors declare that they have no known competing financial interests or personal relationships that could have appeared to influence the work reported in this paper.

Funding

This work was supported by National key research and development program of China (2022YFF1102500).

Appendix A. Supplementary data

Supplementary data associated with this article can be found, in the online version, at http://doi.org/10.26599/FSHW.2024.9250364.

References

[1] J. Zheng, M. Li, B. Tang, et al., Levels, spatial distribution, and impact factors of heavy metals in the hair of metropolitan residents in China and human health implications, Environ. Sci. Technol. 55 (2021) 10578-10588. https://doi.org/10.1021/acs.est.1c02001.

[2] S. Fujimaki, N. Suzui, N.S. Ishioka, et al., Tracing cadmium from culture to spikelet: noninvasive imaging and quantitative characterization of absorption, transport, and accumulation of cadmium in an intact rice plant, Plant Physiol. 152 (2010) 1796-1806. https://doi.org/10.1104/pp.109.151035.

[3] L. Tang, Y. Hamid, D. Liu, et al., Foliar application of zinc and selenium alleviates cadmium and lead toxicity of water spinach-bioavailability/cytotoxicity study with human cell lines, Environ. Int. 145 (2020) 106122. https://doi.org/10.1016/j.envint.2020.106122.

[4] W. Tian, M.Y. Zhang, D.P. Zong, et al., Are high-risk heavy metal(loid)s contaminated vegetables detrimental to human health? A study of incorporating bioaccessibility and toxicity into accurate health risk assessment, Sci. Total Environ. 897 (2023) 165514. https://doi.org/10.1016/j.scitotenv.2023.165514.

[5] K.L. Harris, L.D. Banks, J.A. Mantey, et al., Bioaccessibility of polycyclic aromatic hydrocarbons: relevance to toxicity and carcinogenesis, Expert Opin. Drug Metab. Toxicol. 9 (2013) 1465-1480. https://doi.org/10.1517/17425255.2013.823157.

[6] Q. Lin, Y. Hamid, H. Wang, et al., Co-foliar application of zinc and nano-silicon to rice helps in reducing cadmium exposure risk: investigations through *in-vitro* digestion with human cell line bioavailability assay, J. Hazard. Mater. 468 (2024) 133822. https://doi.org/10.1016/j.jhazmat.2024.133822.

[7] D. Liu, L. Lu, M. Wang, et al., Tetracycline uptake by pak choi grown on contaminated soils and its toxicity in human liver cell line HL-7702, Environ. Pollut. 253 (2019) 312-321. https://doi.org/10.1016/j.envpol.2019.06.086.

[8] J. Li, Y. Song, R.D. Vogt, et al., Bioavailability and cytotoxicity of cerium-(IV), copper-(II), and zinc oxide nanoparticles to human intestinal and liver cells through food, Sci. Total Environ. 702 (2020) 134700. https://doi.org/10.1016/j.scitotenv.2019.134700.

[9] T. Langerholc, P.A. Maragkoudakis, J. Wollgast, et al., Novel and established intestinal cell line models - an indispensable tool in food science and nutrition, Trends Food Sci. Technol. 22 (2011) S11-s20. https://doi.org/10.1016/j.tifs.2011.03.010.

[10] K.J. Wu, B. Gong, P.C. Wang, et al., Assessment and comparison of bioavailability of cadmium in different foods using *in vitro*, *in cellulo*, and *in vivo* models, Food Anal. Methods. 15 (2022) 2951-2958. https://doi.org/10.1007/s12161-022-02338-8.

[11] B.M. Baker, C.S. Chen, Deconstructing the third dimension: how 3D culture microenvironments alter cellular cues, J. Cell Sci. 125 (2012) 3015-3024. https://doi.org/10.1242/jcs.079509.

[12] K.J. Jang, A.P. Mehr, G.A. Hamilton, et al., Human kidney proximal tubule-on-a-chip for drug transport and nephrotoxicity assessment, Integr. Biol. 5 (2013) 1119-1129. https://doi.org/10.1039/c3ib40049b.

[13] M.E. Johansson, H. Sjövall, G.C. Hansson, The gastrointestinal mucus system in health and disease, Nat. Rev. Gastroenterol. Hepatol. 10 (2013) 352-361. https://doi.org/10.1038/nrgastro.2013.35.

[14] C. Hu, S. Yang, T. Zhang, et al., Organoids and organoids-on-a-chip as the new testing strategies for environmental toxicology-applications & advantages, Environ. Int. 184 (2024) 108415. https://doi.org/10.1016/j.envint.2024.108415.

[15] H.J. Kim, J. Lee, J.H. Choi, et al., Co-culture of living microbiome with microengineered human intestinal villi in a gut-on-a-chip microfluidic device, J. Vis. Exp. 30 (2016) 54344. https://doi.org/10.3791/54344.

[16] Z. Hou, R. Meng, G. Chen, et al., Distinct accumulation of nanoplastics in human intestinal organoids, Sci. Total Environ. 838 (2022) 155811. https://doi.org/10.1016/j.scitotenv.2022.155811.

[17] Y. Wei, X. Zheng, Z. Zhang, et al., *In vivo-in vitro* correlations for the assessment of cadmium bioavailability in vegetables, J. Agric. Food Chem. 69 (2021) 12295-12304. https://doi.org/10.1021/acs.jafc.1c03284.

[18] A.G. Oomen, C.J. Rompelberg, M.A. Bruil, et al., Development of an *in vitro* digestion model for estimating the bioaccessibility of soil contaminants, Arch. Environ. Contam. Toxicol. 44 (2003) 281-287. https://doi.org/10.1007/s00244-002-1278-0.

[19] M.E.V. Johansson, D. Ambort, T. Pelaseyed, et al., Composition and functional role of the mucus layers in the intestine, Cell. Mol. Life Sci. 68 (2011) 3635-3641. https://doi.org/10.1007/s00018-011-0822-3.

[20] A. Schepers, C. Li, A. Chhabra, et al., Engineering a perfusable 3D human liver platform from iPS cells, Lab Chip 16 (2016) 2644-2653. https://doi.org/10.1039/c6lc00598e.

[21] C. Li, Y. Sun, T. He, et al., Synergistic effect of lactoferrin and osteopontin on intestinal barrier injury, Int. J. Biol. Macromol. 253 (2023) 127416. https://doi.org/10.1016/j.ijbiomac.2023.127416.

[22] X. Deng, G. Zhang, C. Shen, et al., Hollow fiber culture accelerates differentiation of Caco-2 cells, Appl. Microbiol. Biotechnol. 97 (2013) 6943-6955. https://doi.org/10.1007/s00253-013-4975-x.

[23] E. Sciurti, L. Blasi, C.T. Prontera, et al., TEER and ion selective transwell-integrated sensors system for Caco-2 cell model, Micromachines 14 (2023) 496. https://doi.org/10.3390/mi14030496.

[24] R. Aziz, M.T. Rafiq, T. Li, et al., Uptake of cadmium by rice grown on contaminated soils and its bioavailability/toxicity in human cell lines (Caco-2/HL-7702), J. Agric. Food Chem. 63 (2015) 3599-3608. https://doi.org/10.1021/jf505557g.

[25] Q. Lin, Y. Hamid, H. Yang, et al., Cadmium mobility and health risk assessment in the soil-rice-human system using *in vitro* biaccessibility and *in vivo* bioavailability assay: two year field experiment, Sci. Total Environ. 867 (2023) 161564. https://doi.org/10.1016/j.scitotenv.2023.161564.

[26] L. Yang, X. Zhang, D. Zhao, et al., Relative bioavailability of cadmium in rice: assessment, modeling, and application for risk assessment, Foods 12 (2023) 984. https://doi.org/10.3390/foods12050984.

[27] P.G. Reeves, R.L. Chaney, Marginal nutritional status of zinc, iron, and calcium increases cadmium retention in the duodenum and other organs of rats fed rice-based diets, Environ. Res. 96 (2004) 311-322. https://doi.org/10.1016/j.envres.2004.02.013.

[28] Q. Lv, Q. He, Y. Wu, et al., Investigating the bioaccessibility and bioavailability of cadmium in a cooked rice food matrix by using an 11-day rapid Caco-2/HT-29 co-culture cell model combined with an *in vitro* digestion model, Biol. Trace Elem. Res. 190 (2019) 336-348. https://doi.org/10.1007/s12011-018-1554-0.

[29] S. Sun, X.F. Zhou, Z. Li, et al., *In vitro* and *in vivo* testing to determine Cd bioaccessibility and bioavailability in contaminated rice in relation to mouse chow, Int. J. Environ. Res. Public Health. 16 (2019) 871. https://doi.org/10.3390/ijerph16050871.

[30] W. Shin, H.J. Kim, 3D *in vitro* morphogenesis of human intestinal epithelium in a gut-on-a-chip or a hybrid chip with a cell culture insert, Nat. Protoc. 17 (2022) 910-939. https://doi.org/10.1038/s41596-021-00674-3.

[31] H.J. Kim, H. Li, J.J. Collins, et al., Contributions of microbiome and mechanical deformation to intestinal bacterial overgrowth and inflammation in a human gut-on-a-chip, PNAS 113 (2016) E7-15. https://doi.org/10.1073/pnas.1522193112.

[32] J. Taelman, M. Diaz, J. Guiu, Human intestinal organoids: promise and challenge, Front. Cell Dev. Biol. 10 (2022) 854740. https://doi.org/10.3389/fcell.2022.854740.

[33] A.S. Fanning, B.J. Jameson, L.A. Jesaitis, et al., The tight junction protein ZO-1 establishes a link between the transmembrane protein occludin and the actin cytoskeleton, J. Biol. Chem. 273 (1998) 29745-29753. https://doi.org/10.1074/jbc.273.45.29745.

[34] S. Nathani, N. Das, P. Katiyar, et al., Consumption of honey ameliorates lipopolysaccharide-induced intestinal barrier dysfunction *via* upregulation of tight junction proteins, Eur. J. Nutr. 62 (2023) 3033-3054. https://doi.org/10.1007/s00394-023-03203-y.

[35] O. Kwon, T.S. Han, M.Y. Son, Intestinal morphogenesis in development, regeneration, and disease: The potential utility of intestinal organoids for studying compartmentalization of the crypt-villus structure, Front. Cell Dev. Biol. 8 (2020) 593969. https://doi.org/10.3389/fcell.2020.593969.

[36] J.J. Dehmer, A.P. Garrison, K.E. Speck, et al., Expansion of intestinal epithelial stem cells during murine development, PloS One 6 (2011) e27070. https://doi.org/10.1371/journal.pone.0027070.

[37] K.D. Sumigray, M. Terwilliger, T. Lechler, Morphogenesis and compartmentalization of the intestinal crypt, Dev. Cell 45 (2018) 183-197. https://doi.org/10.1016/j.devcel.2018.03.024.

[38] J.J. Faust, K. Doudrick, Y. Yang, et al., Food grade titanium dioxide disrupts intestinal brush border microvilli *in vitro* independent of sedimentation, Cell Biol. Toxicol. 30 (2014) 169-188. https://doi.org/10.1007/s10565-014-9278-1.

[39] D. Dutta, I. Heo, H. Clevers, Disease modeling in stem cell-derived 3D organoid systems, Trends Mol. Med. 23 (2017) 393-410. https://doi.org/10.1016/j.molmed.2017.02.007.

[40] S. Miura, A. Suzuki, Brief summary of the current protocols for generating intestinal organoids, Dev. Growth Differ. 60 (2018) 387-392. https://doi.org/10.1111/dgd.12559.

[41] R. Przybylla, M. Krohn, M.L. Sellin, et al., Novel *in vitro* models for cell differentiation and drug transport studies of the human intestine, Cells 12 (2023) 2371. https://doi.org/10.3390/cells12192371.

[42] J. McCright, A. Sinha, K. Maisel, Generating an *in vitro* gut model with physiologically relevant biophysical mucus properties, Cell. Mol. Bioeng. 15 (2022) 479-491. https://doi.org/10.1007/s12195-022-00740-0.

[43] A. Macierzanka, A.R. Mackie, L. Krupa, Permeability of the small intestinal mucus for physiologically relevant studies: impact of mucus location and *ex vivo* treatment, Sci. Rep. 9 (2019) 17516. https://doi.org/10.1038/s41598-019-53933-5.

[44] S.Y. Lee, Y. Lee, N. Choi, et al., Development of gut-mucus chip for intestinal absorption study, BioChip J. 17 (2023) 230-243. https://doi.org/10.1007/s13206-023-00097-0.

[45] I. Sabolić, D. Breljak, M. Škarica, et al., Role of metallothionein in cadmium traffic and toxicity in kidneys and other mammalian organs, BioMetals 23 (2010) 897-926. https://doi.org/10.1007/s10534-010-9351-z.

[46] R.V. McNeill, A.S. Mason, M.E. Hodson, et al., Specificity of the metallothionein-1 response by cadmium-exposed normal human urothelial cells, Int. J. Mol. Sci. 20 (2019) 1344. https://doi.org/10.3390/ijms20061344.

[47] W. Xiao, Y. Yang, N. Tang, et al., Innovative accumulative risk assessment of co-exposure to Cd, As, and Pb in contaminated rice based on their *in vivo* bioavailability and *in vitro* bioaccessibility, Sci. Total Environ. 912 (2024) 168922. https://doi.org/10.1016/j.scitotenv.2023.168922.

[48] X. Zheng, Z. Zhang, J. Chen, et al., Comparative evaluation of *in vivo* relative bioavailability and *in vitro* bioaccessibility of arsenic in leafy vegetables and its implication in human exposure assessment. J. Hazard Mater. 423(Pt A) (2022) 126909. https://doi.org/10.1016/j.jhazmat.2021.126909.

[49] P. Zhuang, S. Sun, X.F. Zhou, et al., Bioavailability and bioaccessibility of cadmium in contaminated rice by *in vivo* and *in vitro* bioassays, Sci. Total Environ. 719 (2020) 137453. https://doi.org/10.1016/j.scitotenv.2020.137453.

[50] S.W. Li, H.J. Sun, H.B. Li, et al., Assessment of cadmium bioaccessibility to predict its bioavailability in contaminated soils, Environ. Int. 94 (2016) 600-606. https://doi.org/10.1016/j.envint.2016.06.022.

[51] D. Zhao, P. Wang, F.J. Zhao, Dietary cadmium exposure, risks to human health and mitigation strategies, Crit. Rev. Env. Sci. Tec. 53(8) (2023) 939-963. https://doi.org/10.1080/10643389.2022.2099192.

[52] A. Fatehullah, S. Sharma, I.P. Newton, et al., Increased variability in $Apc^{Min/+}$ intestinal tissue can be measured with microultrasound, Sci. Rep. 6 (2016) 29570. https://doi.org/10.1038/srep29570.

[53] L.J. Broutier, G. Mastrogiovanni, M.M.A. Verstegen, et al., Human primary liver cancer-derived organoid cultures for disease modelling and drug screening, Nat. Med. 23 (2017) 1424-1435. https://doi.org/10.1038/nm.4438.

[54] Y.E. Bar-Ephraim, K. Kretzschmar, H. Clevers, Organoids in immunological research, Nat. Rev. Immunol. 20 (2020) 279-293. https://doi.org/10.1038/s41577-019-0248-y.

[55] M.S. Jeon, Y.Y. Choi, S.J. Mo, et al., Contributions of the microbiome to intestinal inflammation in a gut-on-a-chip, Nano Converg. 9 (2022) 8. https://doi.org/10.1186/s40580-022-00299-6.

[56] H.J. Kim, D. Huh, G. Hamilton, et al., Human gut-on-a-chip inhabited by microbial flora that experiences intestinal peristalsis-like motions and flow, Lab Chip 12 (2012) 2165-2174. https://doi.org/10.1039/c2lc40074j.

[57] M. Wang, Y. Sasaki, R. Sakagami, et al., Perfluoropolyether-based gut-liver-on-a-chip for the evaluation of first-pass metabolism and oral bioavailability of drugs, ACS Biomater. Sci. Eng. 10 (2024) 4635-4644. https://doi.org/10.1021/acsbiomaterials.4c00605.

[58] C. Beaurivage, A. Kanapeckaite, C. Loomans, et al., Development of a human primary gut-on-a-chip to model inflammatory processes, Sci. Rep. 10 (2020) 21475. https://doi.org/10.1038/s41598-020-78359-2.